2012: The Journal of Astronomical Data 18, 3.

Infrared extinction spectra of aerosols with relevance to planetary and lunar atmospheres. I: Single-component aerosols

Kerry J. Knox, E. Kathrin Lang and Ruth Signorell*
Department of Chemistry, University of British Columbia,
2036 Main Mall, Vancouver, British Columbia V6T 1Z1, Canada
* Corresponding author: Telephone: +1 604 822-9064, Fax: +1 604 822-2847
e-mail: signorell@chem.ubc.ca

Received December 19, 2011, accepted February 16, 2012

Abstract

Mid-infrared extinction spectra (500–6000 cm^{-1}) of a series of single-component aerosol particle ensembles representative of those found in a range of planetary and lunar atmospheres are presented. The aerosols were generated in the laboratory *via* condensation from the gas phase in a bath gas cooling cell, and the spectra recorded using a Fourier transform infrared spectrometer. This paper is the first in a series aimed towards building a spectral database for use in remote sensing of aerosols. The aerosol substances included here are methane, ethane, propane, butane, pentane, ethylene, acetylene, carbon dioxide, ammonia and sulfur dioxide.

Keywords: Vibrational spectroscopy, cloud condensates, planets and satellites

1 Introduction

Aerosols and clouds are a feature of a wide range of planetary and lunar atmospheres, for example those of Mars, Jupiter, Saturn, Saturn's moon Titan, Uranus and Neptune (Courtin 2005, Montmessin et al. 2007, de Kok et al. 2007, Tomasko et al. 2005, Lindal et al. 1987, Max et al. 2003). There remains considerable uncertainty surrounding the physical and optical properties of aerosol particles and cloud condensates (McKay et al. 2001, Fletcher et al. 2009, Orton et al. 2009, Hofstadter et al. 2009). This uncertainty leads to difficulty in determining the abundances, distributions and roles of aerosols and clouds in the relevant climate systems. The uncertainty can also greatly complicate, and limit the accuracy of,

the retrieval of information from remote sensing data and atmospheric modeling studies (Fletcher et al. 2007, Rodriguez et al. 2003).

While measurements on thin films and bulk samples can be used to determine the characteristic spectral fingerprint of a given substance, such measurements cannot account for the effects of particle properties, for example shape and morphology, on aerosol spectra. Through a combination of laboratory measurements and novel theoretical approaches, Signorell and co-workers have developed a thorough understanding of the molecular basis for the characteristic spectral signatures of aerosol particles in the mid-infrared (mid-IR) (Sigurbjörnsson et al. 2009). Through this work it has been demonstrated that mid-IR spectra can be used to determine a range of the physical properties of aerosols, for example particle shape, morphology, phase and crystal structure (Kunzmann et al. 2001, Bonnamy et al. 2003, Kunzmann et al. 2003, Signorell 2003a,b, Signorell & Kunzmann 2003, Jetzki et al. 2004, Bonnamy et al. 2005, Firanescu et al. 2006a, Firanescu et al. 2006b, Signorell et al. 2006, Signorell & Jetzki 2007, Firanescu et al. 2008, Signorell & Jetzki, M. 2008, Sigurbjörnsson et al. 2009, Wang et al. 2009, Preston et al. 2010). Briefly, the laboratory measurements involve the generation of aerosol ensembles in a custom-built cooling cell, the conditions within which can be tuned to represent a range of lunar and planetary atmospheres (Signorell 2003a, Firanescu et al. 2006a). Once generated, mid-IR absorption spectra of the particle ensembles are recorded in transmission using a Fourier transform spectrometer. The theoretical approaches used to rationalize the collected spectra include vibrational exciton calculations, density functional calculations, and molecular dynamics and Monte Carlo simulations.

As mid-IR spectra can be used to elucidate aerosol properties, it follows that such information can contribute to reducing the uncertainty surrounding aerosol physical and optical properties in astronomical studies, and also to account for the effect of aerosol extinction on planetary processes. Provided the factors affecting aerosol spectra are understood, such spectra can be used to detect and characterize aerosols in planetary atmospheres. Laboratory spectra are therefore collected here as machine-readable data for a range of aerosols relevant to planetary and lunar atmospheres such as those mentioned above, with the aim of providing a convenient source of reference data for astrophysical studies. Wherever relevant, spectra characteristic of several phases and crystal structures for each given substance are presented. The spectra presented here are for single-component aerosol particles; spectra for mixed-composition particles will follow in a subsequent publication. In most cases a detailed analysis of the molecular basis of the characteristic spectral signatures is available in a previous publication, while in the case of a few substances this will be the subject of future contributions.

The substances for which aerosol spectra are presented in this manuscript are listed in Table 1, along with the normal melting point (at 1 atmosphere) of the substance and examples of atmospheric environments in which such particles are thought or have been confirmed to be present. The data are provided for the spectral region from around 500 to 6000 cm^{-1}, with the exact range presented varying slightly for each data set. This range includes the 4.6 to 5.8 μm window useful for observations of methane-rich atmospheres such as that of Titan (Atreya et al. 2006).

2 Experimental

A brief summary of the experimental set-up is provided here; detailed descriptions can be found elsewhere (Firanescu et al. 2006a, Signorell 2003a). Ensembles of single-component aerosols were generated by injecting a warm (temperature = 292 K) gas-phase sample of the aerosol substance of interest into a cold bath gas present in a custom-built cooling cell (temperature of the bath gas: 4–95 K). Supersaturation of the sample gas in the cell leads to particle formation. In these measurements the particles typically vary in size from a few tens to several hundreds of nanometers in diameter; in general the particle size increases with time after formation. The particle number concentration in the cell is typically $\sim 10^4$ to 10^9 cm^{-3}. The temperature, pressure and gas-phase composition in the cooling cell can be controlled, and hence it is possible to simulate the conditions present in a wide range of planetary and lunar atmospheres. Liquid helium or nitrogen is used as a coolant, and heaters are employed to access temperatures above the coolant boiling point.

Mid-IR absorption spectra of the aerosol ensembles were recorded in transmission in the region from approximately 500 to 6000 cm^{-1} using a rapid-scan Fourier transform infrared (FTIR) spectrometer (Bruker IFS 66v/S). The spectral resolutions used in these measurements were between 0.25 and 1 cm^{-1}. The IR light beam was provided by a Globar light source and makes multiple passes through the cell *via* a set of White optics (White 1942), resulting in a total path length of up to several meters, before being transferred to a mercury-cadmium-telluride detector (InfraRed Associates).

The substances used were of purities $> 99.98\%$ and were used as supplied, with the exception of acetylene which was supplied with a purity of 99.6% and which was purified by freezing out the stabilizer prior to use. Pentane was supplied as a spectroscopic grade liquid. In the spectra presented here the bath gas was either nitrogen or helium; in some cases aerosol phase changes are observed to proceed more rapidly in helium than nitrogen (Wang et al. 2010, Lang et al. 2011), and hence the choice of the bath gas was determined by the dynamics of the relevant phase changes and the measurement timescale, with the objective of observing as many aerosol phases and/or crystal structures as possible. The aerosol substances were injected into the cell diluted by a factor of around 10^3 in the major bath gas present in the cell.

The spectra were recorded at time intervals of between 2 and 200 seconds, starting immediately after particle formation and continuing for a total time of around 40 to 120 minutes. Longer measurement times cannot be realized using this measurement scheme because of diffusion of the aerosol particles out of the IR light beam; this also results in the recorded IR signals becoming weaker over time.

3 Spectra of pure aerosols

Table 2 lists the aerosol spectral data files which accompany this manuscript as machine-readable data, along with the dominant aerosol phase or crystal structure sampled, the time

after injection of gases at which the spectrum was recorded, the bath gas used, the temperature at which the spectrum was recorded and the spectral range presented. As the spectra are collected for an aerosol ensemble, it is often the case that the spectrum represents a sum of contributions from two or more phases. The spectra have been provided in their original form, without any attempt to separate out the contributions from each phase, as such a task would require assumptions about the abundance and size distribution of particles in each phase. Each spectral data set has been normalized relative to the largest peak present in the spectrum arising from the substance of interest (i.e. neglecting impurities).

For measurements performed in a bath gas of nitrogen at temperatures close to the boiling point of nitrogen, it is observed that nitrogen is incorporated into liquid aerosol particles, but is excluded as they crystallize (Wang et al. 2010, Lang et al. 2011, Firanescu et al. 2011). The consequences of this phenomenon for the aerosol spectra are discussed in Section 4. It is not expected that helium is incorporated into the particles for measurements carried out at temperatures of around 78 K.

In certain cases weak signals are observed around 3200 cm^{-1} and 2360 cm^{-1}. These signals arise from trace water and carbon dioxide, respectively, and are the result of small amounts of ambient air entering the optical path or the gas samples during their preparation, or, in the case of the signal at 3200 cm^{-1}, from the occurrence of water-ice on the window of the cooled detector.

The presented spectra were recorded at varying times after the injection of gas into the cell, depending upon the aerosol phase of interest. As well as often changing phase, the particles also tend to increase in size with increasing time after formation, which gives rise to the increasingly-slanted baselines observed in the recorded spectra, a result of elastic scattering of light by large particles (Bohren & Huffmann 1998). The presented spectra have not been corrected for such scattering signatures. Owing to the contribution of scattering to light attenuation by particles, the presented data are extinction, rather than absorption, spectra. Extinction is the attenuation of light by absorption and scattering by particles and is defined, in the same way as absorbance, as $\log_{10}(I_o/I)$, where I_o is the light incident on the sample and I is the light transmitted through the sample.

In most cases the spectral data have been discussed in detail in previous publications (as indicated in Table 2), or will be the subject of future publications (in the case of propane, butane and pentane). Therefore only a brief summary of pertinent experimental or analytical details are provided here for each of the aerosol substances presented. A graphical representation of the aerosol spectra has been provided as in the case of methane aerosols (Figures 1 and 2) for illustrative purposes. Where precise band positions are provided they refer to the position of maximum peak intensity.

3.1 Methane

The mid-IR extinction spectra of solid methane aerosols in three phases were measured by Signorell and Jetzki in 2007 (Signorell & Jetzki 2007). The average particle radius was $\sim$ 5 nm, and the particle number concentration $\sim 10^9$ cm^{-3}. The particles were generated

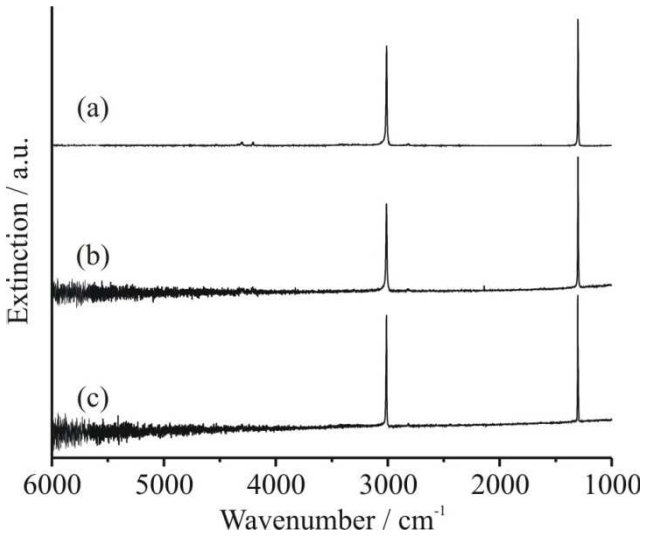

Figure 1: IR extinction spectra of solid methane aerosols for particles consisting of (a) amorphous methane, $T < 91$ K; (b) phase I methane, 20.4 K $< T <$ 91 K; (c) a core of phase II methane with phase I methane present at the surface, $T = 8$ K. The slanted baseline in this spectrum arises from light scattering by large particles (Bohren & Huffmann 1998).

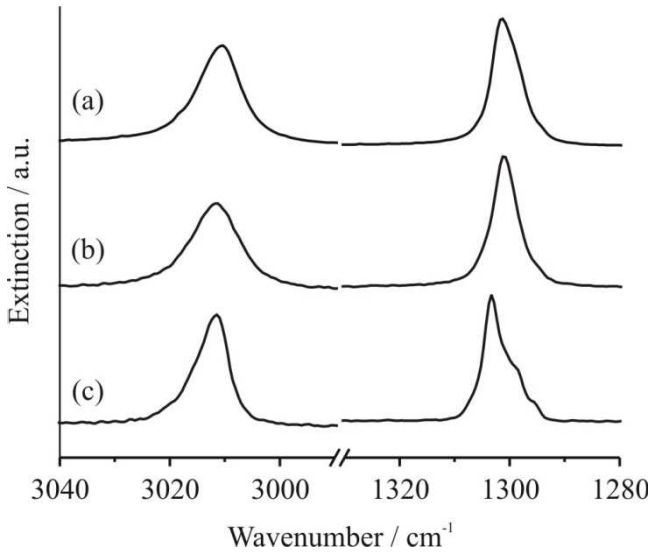

Figure 2: IR extinction bands (ν_3 at $\sim 3010\,\mathrm{cm}^{-1}$ and ν_4 at $\sim 1300\,\mathrm{cm}^{-1}$) of solid methane aerosols for particles consisting of (a) amorphous methane, $T < 91$ K; (b) phase I methane, 20.4 K $< T <$ 91 K; (c) a core of phase II methane with phase I methane present at the surface, $T = 8$ K.

in a bath gas of helium. The normalized spectra are provided from 1000 to 6000 cm^{-1} and are presented graphically in Figure 1. The two IR absorption bands observed arise from excitation of the triply degenerate stretching mode ν_3 at $\sim$ 3010 cm^{-1} and the triply degenerate bending mode ν_4 at $\sim$ 1300 cm^{-1}. The three spectra shown in Figure 1 are for particles consisting of (a) amorphous methane, temperature (T) $<$ 91 K (ch4_1); (b) phase I methane, 20.4 K $<$ T $<$ 91 K (ch4_2); (c) a core of phase II methane with phase I methane present at the surface, T = 8 K (ch4_3).

Figure 2 shows the ν_3 and ν_4 bands in more detail. The shapes of the bands are characteristic of particles in a given phase, as has been determined by comparison with theory (Signorell & Jetzki 2007). For example, the unstructured, slightly asymmetric bands shown in part (a) are characteristic of particles consisting of amorphous methane, the symmetric bands in part (b) are characteristic of particles consisting of phase I methane, and the structured peaks with shoulders in part (c) are characteristic of particles consisting of a combination of phase I and phase II methane. The slanted baseline in this spectrum arises from light scattering from large particles (Bohren & Huffmann 1998); this effect can be observed in many of the spectra presented here, often to a greater extent, which indicates that even larger particles are present.

3.2 Ethane

The particle phase dependence of the mid-IR extinction spectrum of ethane aerosols has been discussed in detail in previous publications (Sigurbjörnsson & Signorell 2008, Wang et al. 2010, Lang et al. 2011). Briefly, upon injection of ethane gas into the cell, which is held at 78 K, supercooled liquid ethane droplets are formed which freeze over time. The spectra provided were recorded with increasing time after injection of ethane into the cell, and hence chart the progressive freezing of the ethane particles. The spectra c2h6_1, c2h6_2 and c2h6_3 correspond to supercooled liquid particles, combined phase I and phase II particles, and phase II particles, respectively. It has not been attempted to separate the contributions from the different phases in spectrum c2h6_2; difference spectra representative of phase I and II ethane aerosols have however been provided elsewhere (Lang et al. 2011).

In particular the ν_8, ν_6 and ν_9 ethane bands, at 1463, 1370, and 819 cm^{-1}, respectively, are sensitive to the particle phase; of these the narrow features of the ν_9 band for solid ethane make this band particularly useful for distinguishing between spectra arising from liquid and solid particles.

c2h6_1 to c2h6_3 were recorded using a relatively high concentration of ethane in the cooling cell. The relatively weak absorption bands around 1600 to 600 cm^{-1} are highly sensitive to phase, and using a high concentration of ethane allows the features of these bands to be examined in detail. The relatively strong absorption band at around 3000 cm^{-1} is however saturated at this concentration of ethane, and hence these spectra are only provided from 2800 to 600 cm^{-1}. The band at around 3000 cm^{-1} is insensitive to particle phase; a spectrum for supercooled liquid ethane particles is provided as c2h6_4, recorded with a lower concentration of ethane in the cell at which this band is not saturated. In spectrum c2h6_4, the broad weak signal observed around 3200 cm^{-1} arises from trace water which

resulted from small amounts of water contaminating the gas sample during its preparation, or possibly from the occurrence of water-ice on the window of the cooled detector. Finally, c2h6_5 is the same spectrum as c2h6_1, however provided for a wider spectral range of 6000 to 600 cm^{-1}. Although the band at around 3000 cm^{-1} is saturated in this spectrum, owing to the high concentration of ethane in the cell, several relatively weak ethane bands in the region from 4500 to 3200 cm^{-1} can be observed under these conditions. This region is useful for ground-based observations as it overlaps with the spectral window in the atmosphere of Earth centered at around 2.2 μm (Larson 1980).

3.3 Propane

Propane has certain properties which are unusual among the alkanes: it has an anomalously low melting point (Boese et al. 1999, Thalladi & Boese 2000), and it has been observed that an anomalously high degree of supercooling is possible in bulk samples before crystallization occurs (Maass & Wright 1921, Snyder & Schachtschneider 1963, Pavese & Besley 1981). The spectra of liquid propane particles (measured above the melting point, at $\sim$ 95 K), and of propane particles below the melting point are presented here, as c3h8_1 and c3h8_2, respectively. It should be noted that the fluctuations in the baseline of the warm spectrum (c3h8_1) result from temperature instabilities of the sample and optics which arise as a result of introducing a heat source to the experimental chamber. In these spectra, the broad weak signal observed around 3200 cm^{-1} again arises from trace water contaminating the gas sample, or possibly from the occurrence of water-ice on the window of the cooled detector.

It can be seen that the bands in this pair of spectra match very closely, and further, a double-peaked feature at 1460 cm^{-1} which has previously been observed in measurements on thin films of crystalline propane (Coustenis et al. 1999) is not present in the aerosol spectrum. It is therefore reasoned that the spectrum c3h8_2 arises from either supercooled liquid, highly viscous, or amorphous, rather than crystalline propane particles. Indeed, despite considerable efforts, and under a range of conditions, crystallization of propane particles has not been observed in these measurements. The anomalously slow crystallization of propane aerosols will be discussed in more detail in a forthcoming publication (Lang et al. 2012a).

3.4 nButane

n-Butane has a melting point of 135 K, and hence it is likely that the aerosol particles condense directly to the solid state upon introduction of n-butane gas to the cell when at 78 K. That the particles are solid immediately after injection of gas to the cell is supported by the observation that the bands in the earliest spectrum after gas injection, c4h10_1, match closely with those reported by Axford and Rank for solid n-butane at $\sim$ 78 K; in particular the bands at 1233 and 1133 cm^{-1} which are characteristic of liquid n-butane are missing (Axford, D.W.E. and Rank, D.H. 1949). Three phases of n-butane aerosols were observed in these measurements. Spectra are provided for each of the three phases observed, following the assignment of Cangeloni et al.: the observed absorption bands present in the spectra c4h10_1, c4h10_2 and c4h10_3 match closely with those in the spectra attributed by

Cangeloni et al. to a solid disordered phase ("phase I", 108 K), a metastable monoclinic phase ("phase II", 77 K), and a triclinic phase ("phase III", 77 K), respectively (Cangeloni, M.L. and Schettino, V. 1975), although it should be noted that in c4h10_2 weak features of phase I are still present. Detailed spectral assignment and analysis of the kinetics of the phase transitions of butane aerosols will be the subject of a forthcoming publication (Lang, E.K. et al. 2012b). In these spectra, the broad signals observed around 3200 cm^{-1} and 2360 cm^{-1} arise from trace ambient air entering the optical path, and potentially from trace water contamination in the gas sample.

3.5 n-Pentane

Similarly to n-butane, n-Pentane has a high melting point (143 K), and hence it is likely that the aerosol particles condense directly to the solid state upon introduction of n-pentane gas to the cell when at 78 K. That the particles are solid immediately after injection of gas to the cell is again supported by the observation that the bands in the earliest spectrum after gas injection, c5h12_1, match closely with those reported for solid n-pentane at $\sim$ 78 K by Axford and Rank (Axford, D.W.E. and Rank, D.H. 1950). For example, the bands at 1342 and 907 cm^{-1} which are characteristic of liquid n-pentane are missing. A single phase transition is observed under these conditions, reasoned to be that from a disordered solid state (likely amorphous solid rather than supercooled liquid, as discussed above) (c5h12_1) to a crystalline phase (c5h12_2). The bands around 1460 and 1380 cm^{-1} are particularly useful for distinguishing between spectra arising from particles in differing phases. The spectral features of pentane aerosols and the kinetics of this phase transition will be discussed in detail in a forthcoming publication (Lang, E.K. et al. 2012a). In these spectra a broad signal is observed around 3200 cm^{-1}, arising from trace water contaminating the gas sample, or from the occurrence of water-ice on the window of the cooled detector.

If a higher concentration of pentane is present in the cell, soon after particle formation (c5h12_3), spectral features consistent with the presence of at least two conformational isomers of pentane are observed. As the observed phase transition proceeds, several of these spectral features are lost (c5h12_4), reasoned to be those associated with less stable rotamers. Several of the bands which are lost, for example the bands at 1238 and 908 cm^{-1}, coincide with those attributed to less stable rotamers of liquid pentane in vibrational studies (Snyder, R.G. 1967, Keefe, C.D. and Jaspers-Fayer, S. 2011) and calculations (Mirkin, N.G. and Krimm, S. 2000). These observations would be consistent with initial fixing of unstable rotamers during rapid freezing to an amorphous state, followed by conversion to the stable anti rotamers, as has previously been observed in work using matrix-isolated alkanes by Goodman et al. (Goodman, M.A. et al. 1983). This process and the relevant spectral assignments will be discussed in detail in a forthcoming publication (Lang, E.K. et al. 2012a).

3.6 Ethylene / ethene

The particle phase dependence of the mid-IR extinction spectrum of ethylene aerosols has been discussed in detail in a previous publication (Wang et al. 2009). Briefly, upon injection

of ethylene into the cell, which contains 900 mbar helium held at 78 K, supercooled liquid ethylene droplets are formed which freeze over time. The normalized spectra provided from 600 to 5000 cm^{-1} as c2h4_1, c2h4_2 and c2h4_3 were recorded at increasing times after injection of ethylene into the cell, and hence represent the progressive freezing of ethylene particles. The spectra c2h4_1, c2h4_2 and c2h4_3 correspond to supercooled liquid particles, combined metastable "a-structure" and stable $P2_1/n$ "b-structure" particles, and particles composed almost entirely of ethylene in the $P2_1/n$ "b-structure", respectively. The band arising from excitation of the CH_2-scissor vibration ν_{12} at $\sim 1440\ cm^{-1}$ is particularly useful for determining the phase of ethylene particles. It should be noted that signatures of gas phase ethylene can be seen in these spectra, and that these affect the appearance of the aerosol bands, particularly in the region around 950 cm^{-1}.

3.7 Acetylene / ethyne

The mid-IR absorption spectra of solid acetylene aerosols in two crystal structures for temperatures between 78 K and 110 K were reported and rationalized by Preston et al. in 2010 (Preston, T.C. et al. 2010). In this work the particle diameters were between $\sim$ 50 and 500 nm, and the particle number concentrations between 10^4 and $10^6\ cm^{-3}$.

The two spectra presented as c2h2_1 and c2h2_2 are for particles consisting of polycrystalline acetylene and orthorhombic crystalline acetylene (produced by annealing polycrystalline particles by condensing ethane onto them), respectively. The spectra are consistent with particles in a globular shape. The two strong IR absorption bands attributable to acetylene arise from excitation of the antisymmetric CH-stretching vibration ν_3, at $\sim 3230\ cm^{-1}$, and the bending vibration ν_5, at $\sim 770\ cm^{-1}$, while the weaker band at $\sim 1390\ cm^{-1}$ is assigned to the $\nu_4 + \nu_5$ combination band (Dunder, T. and Miller, R.E. 1990). In the crystalline state the ν_5 band is strongly influenced by the particle shape (Preston, T.C. et al. 2010). The additional features apparent in spectrum c2h2_2 arise from ethane, which is used to anneal the polycrystalline particles to a crystalline structure.

3.8 Carbon dioxide

The mid-IR extinction spectra of solid carbon dioxide aerosols (cubic crystal structure) have been reported and rationalized by Signorell and co-workers (Signorell 2003b, Signorell & Kunzmann 2003, Signorell et al. 2006, Sigurbjörnsson et al. 2009, Wang et al. 2009, Preston & Signorell 2011). The absorption bands of carbon dioxide depend strongly on particle size, shape and morphology. Here the spectra of solid carbon dioxide aerosols with two particle shapes are presented. The aerosols were generated in a bath gas of nitrogen. The spectra, normalized to the intensity of the band at $\sim 2360\ cm^{-1}$, are provided from 500 to 4500 cm^{-1}. The spectra, co2_1 and co2_2, are characteristic of crystalline particles in the shape of truncated cubes (Preston & Signorell 2011) and with an elongated particle geometry, respectively, as has been previously determined by modeling (Signorell & Kunzmann 2003). It has been observed that a higher pressure in the cell favors the formation of cube-like particles, while a lower pressure favors an elongated particle geometry (Signorell & Kunzmann 2003, Taraschewski et al. 2005).

The two IR absorption bands observed arise from excitation of the antisymmetric stretching mode ν_3, at ~ 2360 cm^{-1} and the bending mode ν_2, at ~ 770 cm^{-1}. The band at 2283 cm^{-1} arises from $^{13}CO_2$; it is not sensitive to particle shape as a result of the low abundance of ^{13}C (1.1 %) (Signorell & Kunzmann 2003). Weak bands at ~ 3600 and ~ 3700 cm^{-1} arise from excitation of the combination vibrations $2\nu_2 + \nu_3$ and $\nu_1 + \nu_3$,respectively.

3.9 Ammonia

The effects of particle shape, surface phenomena and particle size on the mid-IR absorption spectra of solid ammonia aerosols have been previously reported by Signorell and coworkers (Jetzki et al. 2004, Firanescu et al. 2006b). Here spectra of solid crystalline ammonia aerosols which were generated in a bath gas of helium are presented. The spectra nh3_1 and nh3_2 were recorded at varying times after particle formation. As is the case for carbon dioxide aerosols, over time the particles become more elongated in shape. The spectra therefore correspond to varying mixtures of particles with a globular or elongated shape: the features of nh3_1 are dominated by globular shaped particles, while nh3_2 is dominated by particles with an elongated geometry. In the case of ammonia aerosols only the ν_2 band at 1067 cm^{-1} is sensitive to particle shape.

Spectra nh3_1 and nh3_2 correspond to particles with diameters greater than ~ 10 nm, for which surface effects are negligible. For particles with sizes below 10 nm, however, surface effects (and hence particle size) play an important role in determining the spectral signatures. By varying the temperature in the cooling cell, it is possible to control the size of the particles which are formed. nh3_3, nh3_4 and nh3_5 were recorded at cell temperatures of 80 K, 37 K and 21 K, respectively, and correspond to particles with a diameter of ~ 10 nm, 4 nm and 2 nm, respectively (Jetzki, M. et al. 2004). Size-dependent features can be observed in the spectra both in the region of the ν_2 band and the region around 3300 cm^{-1}.

3.10 Sulfur dioxide

The mid-IR absorption spectra of solid sulfur dioxide aerosols have been reported by Signorell and co-workers (Signorell, R. and Jetzki, M. 2008). The average particle diameter was ~ 50 nm, and the particle number concentration $\sim 10^6$ cm^{-3}. The particles were generated in a bath gas of helium. The spectra, normalized to the intensity of the band at 1335 cm^{-1}, are provided from 600 to 5000 cm^{-1}. Detailed modeling and experimental investigations demonstrated that the spectra, so2_1 and so2_2, are consistent with particles which are partially amorphous (observed for $60 < T < 90$ K) and amorphous (observed for $T <$ 10 K), respectively. For these spectra the baseline has been corrected to compensate for the effect of carrying out measurements at varying temperatures.

The two IR absorption bands, observed at 1335 cm^{-1} and 1149 cm^{-1}, arise from excitation of the antisymmetric stretching vibration ν_3 and the symmetric stretching vibration ν_1, respectively. Absorption bands of the isotopomer $^{34}SO_2$ appear to the low wavenumber side of these peaks.

4 Discussion

The uncertainties/stabilities in measured quantities are as follows:

1. Spectral resolution: 0.25 to 1 cm^{-1}.
2. Cell temperature: close to coolant boiling point (4 or 77 K) the temperature is stable to $\pm$ 1 K; far from coolant boiling point the temperature is stable to $\pm$ 5 K.

There are several general factors affecting the collected spectra:

1. For some spectra (i.e. ethane, pentane) recorded in a bath gas of nitrogen at temperatures close to 77 K, it is likely that nitrogen is incorporated into the particles, and that it is excluded during particle crystallization (Wang et al. 2010, Lang et al. 2011, Firanescu et al. 2011). Therefore for several of the liquid (or amorphous) spectra presented here it is important to note that bi-component particles are being sampled. By comparing spectra recorded in bath gases of nitrogen and helium, however, it has been determined that the incorporation of nitrogen does not have a strong effect on the aerosol spectra.
2. These are ensemble measurements, and hence a distribution of particle sizes, shapes, phases and compositions contribute to the recorded spectra. In the sections above situations where more than one particle type contributes strongly to the observed spectra are highlighted.
3. The conditions under which the aerosols exist in planetary and lunar atmospheres can differ from those under which the spectra presented here were recorded. The most stable particle phase and the dynamics of aerosol phase changes are strongly dependent on temperature. The bath gas present (nitrogen or helium) has also been found to be important in determining the rate of aerosol phase changes. In general it has been found that the atmospheric pressure does not have a significant effect on aerosol phase dynamics within the range from 500 to 800 mbar, however it does have an effect on particle shape, for example in the cases of carbon dioxide and ammonia aerosols.

Acknowledgements

Financial support from the Natural Sciences and Engineering Research Council of Canada (NSERC) and the Canada Foundation for Innovation is gratefully acknowledged. K.J.K. acknowledges financial support from the UBC Centre for Aerosol Research and a Killam Postdoctoral Fellowship. E.K.L. acknowledges a graduate fellowship from NSERC through the UBC CREATE-Atmospheric Aerosol Program. R.S. acknowledges a NSERC E.W.R. Steacie Memorial Fellowship. The spectral data collected here are the result of work by a number of researchers, including Drs. Martin Jetzki, Marc K. Kunzmann, Thomas C. Preston, Chia C. Wang, and Philipp Zielke and Mr. Ómar F. Sigurbjörnsson. Modeling work was carried out by Drs. George Firanescu, David Luckhaus and Thomas C. Preston. All are acknowledged for their contributions.

5 Tables

Table 1: Substances for which aerosol spectra are presented, with normal melting points of bulk substances and examples of atmospheres in which the aerosols are thought or have been confirmed to be present.

Aerosol substance	Melting point / K	Examples of relevant atmospheric environments
Methane CH_4	91	Neptune[i–v] Uranus[iv,vi,vii] Titan[iv,vii–x]
Ethane C_2H_6	90	Titan[xi–xiii]
Propane C_3H_8	85	Titan[xiii]
n-Butane C_4H_{10}	135	Titan[xiv,xv]
n-Pentane C_5H_{12}	143	Titan[xvi]
Acetylene C_2H_2	192 (sublimation)	Neptune and Uranus[xvii] Titan[xiii]
Ethylene C_2H_4	104	Titan[xiii]
Ammonia NH_3	195	Jupiter and Saturn[xvii]
Carbon dioxide CO_2	195 (sublimation)	Titan[xiii] Mars[xviii]
Sulfur dioxide SO_2	201	Io and Europa[xix–xxii]

References. *i*: Smith et al. (1989), *ii*: Gibbard et al. (2003), *iii*: Max et al. (2003), *iv*: Sanchez-Lavega et al. (2004), *v*: Karkoschka & Tomasko (2011), *vi*: Lindal et al. (1987), *vii*: Karkoschka & Tomasko (2009), *vii*: Tomasko et al. (2005), *viii*: Fulchignoni et al. (2005), *ix*: Hueso & Sanchez-Lavega (2006), *x*: Tokano et al. (2006), *xi*: Atreya et al. (2006), *xi*: Rannou et al. (2006), *xii*: Griffith et al. (2006), *xiii*: Coustenis et al. (2010), *xiv*: Curtis et al. (2005), *xv*: Lara et al. (1996), *xvi*: Navarro-Gonzalez (et al. 2001), *xvii*: Courtin (2005), *xviii*: Montmessin et al. (2007), *xix*: Sandford & Allamandola (1993), *xx*: Nash & Betts (1995), *xxi*: Schriver-Mazzuoli et al. (2003), *xxii*: Spencer et al. (2005).

Sample of the data: c2h6_1.dat

2799.92782	0.02137
2799.68676	0.02358
2799.44570	0.02313
2799.20464	0.02240
2798.96358	0.02304
2798.72252	0.02372
2798.48145	0.02376
2798.24039	0.02286
2797.99933	0.02099
2797.75827	0.02240
2797.51721	0.02537
2797.27615	0.02370
2797.03509	0.01954
2796.79402	0.01880
2796.55296	0.02139
2796.31190	0.02277
2796.07084	0.02271
2795.82978	0.02251
2795.58872	0.02242
2795.34766	0.02216
2795.10660	0.02025
2794.86553	0.01910
2794.62447	0.02095
2794.38341	0.02212
2794.14235	0.02027
2793.90129	0.01893
2793.66023	0.01900
2793.41917	0.01921
2793.17810	0.02053
2792.93704	0.02181
2792.69598	0.02196
2792.45492	0.01988
2792.21386	0.01825
2791.97280	0.01930
2791.73174	0.02077
2791.49067	0.02286
2791.24961	0.02317
2791.00855	0.02271
2790.76749	0.02242
2790.52643	0.01998
2790.28537	0.01915
2790.04431	0.01908
2789.80324	0.01834
2789.56218	0.01922
2789.32112	0.02056

Table 2: Summary of spectral data presented: ASCII filename, substance & relevant publication(s), dominant particle phase, time relative to injection (s), bath gas pressure (mbar), temperature at which recorded (K), spectral range (cm^{-1}).

File .dat	Substance & references	Dominant particle phase	Time after injection	Bath gas, pressure	Temp. rec.	Spectral range
ch4_1	Methane[a]	Amorphous	0	He, 400	< 91	6000–1000
ch4_2		Crystalline phase I	~ 300		20.4–91	
ch4_3		Crystalline phase I and II	N/A[1]		8	
c2h6_1	Ethane[b,c]	Liquid (supercooled)	1	N_2, 570	78	2800–600
c2h6_2		Phase I and II solid	531			
c2h6_3		Phase II solid	2540			
c2h6_4		Liquid (supercooled)	42	He, 800		6000–600
c2h6_5			1	N_2, 570		
c3h8_1	Propane[d]	Liquid	1098	N_2, 800	95	5000–500
c3h8_2		Liquid (supercooled) or amorphous	10	He, 800	78	5000–500
c4h10_1	n-Butane[e]	Phase I solid	1	N_2, 800	78	6000–600
c4h10_2		Phase II solid	96			
c4h10_3		Phase III solid	5596			
c5h12_1	n-Pentane[d]	Amorphous	0	N_2, 800	78	6000–600
c5h12_2		Crystalline	2534			
c5h12_3		Amorphous	1			1400–800
c5h12_4		Crystalline	5602			
c2h2_1	Acetylene[b,f]	Polycrystalline	1	He, 500–900	79	5000–500
c2h2_2		Crystalline	N/A[2]			
c2h4_1	Ethylene[b]	Liquid (supercooled)	0	He, 900	79	5000–600
c2h4_2		Combination of a and b structures (solid)	1			
c2h4_3		b structure ($P2_1/n$, solid)	86			
co2_1	Carbon dioxide[g–j,b,k]	Truncated cube shape crystalline	1	He, 950	78	4500–500
co2_2		Elongated shape crystalline	50	He, 900		
nh3_1	Ammonia[l,m]	Globular shape crystalline	10	He, 50–1000	80	3600–800
nh3_2		Elongated shape crystalline	884			
nh3_3		10 nm crystalline	N/A		80	3500–800
nh3_4		4 nm crystalline		He, 50–1000	37	
nh3_5		2 nm crystalline			21	
so2_1	Sulfur dioxide[n]	Partially amorphous	0	He, 10–1000	60	5000–600
so2_2		Amorphous	0		< 10	

References. *a*: (Signorell & Jetzki 2007), *b*: Wang et al. (2009), *c*: Lang et al. (2011), *d*: Lang et al. (2012a), *e*: Lang et al. (2012b), *f*: Preston et al. (2010), *g*: Signorell (2003b), *h*: Signorell & Kunzmann (2003), *i*: Signorell et al. (2006), *j*: Sigurbjörnsson et al. (2009), *k*: Preston & Signorell (2011), *l*: Jetzki et al. (2004), *m*: Firanescu et al. (2006b), *n*: Signorell & Jetzki (2008).
Remarks. [1]: after temperature change, [2]: after annealing procedure.

References

Atreya, S.K. et al. 2006, Planetary and Space Science 54, 1177

Axford, D.W.E. & Rank, D.H. 1949, Journal of Chemical Physics 17, 430

Axford, D.W.E. & Rank, D.H. 1950, Journal of Chemical Physics 18, 51

Boese, R. et al. 1999, Angewandte Chemie-International Edition 38, 988

Bohren, C.F. & Huffmann, D.R., 1998, Absorption and Scattering of Light by Small Particles, Wiley-Interscience

Bonnamy, A. et al. 2003, Chemical Physics Letters 382, 547

Bonnamy, A. et al. 2005, Physical Chemistry Chemical Physics 7, 963

Cangeloni, M.L. & Schettino, V. 1975, Molecular Crystals and Liquid Crystals 31, 219

Courtin, R. 2005, Space Science Reviews 116, 185

Coustenis, A. et al. 1999, Planetary and Space Science 47, 1305

Coustenis, A. et al. 2010, Icarus 207, 461

Curtis, D.B. et al. 2005, Journal of Physical Chemistry A 109, 1382

de Kok, R. et al. 2007, Icarus 191, 223

Dunder, T. & Miller, R.E. 1990, Journal of Chemical Physics 93, 3693

Firanescu, G. et al. 2006a, Physical Chemistry Chemical Physics 8, 4149

Firanescu, G. et al. 2006b, Journal of Chemical Physics 125, 144501

Firanescu, G. et al. 2008, Journal of Chemical Physics 128, 184301

Firanescu, G. et al. 2011, Icarus 212, 779

Fletcher, L.N. et al. 2007, Icarus 189, 457

Fletcher, L.N. et al., 2009, Jupiter Atmospheric Science in the Next Decade, Planetary Science Decadal Survey 2013-2023 (white paper)

Fulchignoni, M. et al. 2005, Nature 438, 785

Gibbard, S.G. et al. 2003, Icarus 166, 359

Goodman, M.A. et al. 1983, Journal of Physical Chemistry 87, 1753

Griffith, C.A. et al. 2006, Science 313, 1620

Hofstadter, M. et al., 2009, The Atmospheres of the Ice Giants, Uranus and Neptune, Planetary Science Decadal Survey 2013-2023 (white paper)

Hueso, R. & Sanchez-Lavega, A. 2006, Nature 442, 428

Jetzki, M. et al. 2004, Journal of Chemical Physics 120, 11775

Karkoschka, E. & Tomasko, M. 2009, Icarus 202, 287

Karkoschka, E. & Tomasko, M.G. 2011, Icarus 211, 780

Keefe, C.D. & Jaspers-Fayer, S. 2011, Vibrational Spectroscopy 57, 72

Kunzmann, M.K. et al. 2001, Physical Chemistry Chemical Physics 3, 3742

Kunzmann, M.K. et al. 2003, Spectrochimica Acta Part A-Molecular and Biomolecular Spectroscopy 59, 2855

Lang, E.K. et al. 2011, Planetary and Space Science 59, 722

Lang, E.K. et al. 2012a, in preparation

Lang, E.K. et al. 2012b, in preparation

Lara, L.M. et al. 1996, Journal of Geophysical Research-Planets 101, 23261

Larson, H.P. 1980, Annual Review of Astronomy and Astrophysics 18, 43

Lindal, G.F. et al. 1987, Journal of Geophysical Research-Space Physics 92, 14987

Maass, O. & Wright, C.H. 1921, Journal of the American Chemical Society 43, 1098

Max, C.E. et al. 2003, Astronomical Journal 125, 364

McKay, C.P. et al. 2001, Planetary and Space Science 49, 79

Mirkin, N.G. & Krimm, S. 2000, Journal of Molecular Structure 550, 67

Montmessin, F. et al. 2007, Journal of Geophysical Research-Planets 112, E11S90

Nash, D.B. & Betts, B.H. 1995, Icarus 117, 402

Navarro-Gonzalez, R. et al. 2001, Advances in Space Research 27, 271

Orton, G.S. et al., 2009, Saturn Atmospheric Science in the Next Decade, Planetary Science Decadal Survey 2013-2023 (white paper)

Pavese, F. & Besley, L.M. 1981, Journal of Chemical Thermodynamics 13, 1095

Preston, T.C. et al. 2010, Physical Chemistry Chemical Physics 12, 7924

Preston, T.C. & Signorell, R. 2011, Proceedings of the National Academy of Sciences of the United States of America 108, 5532

Rannou, P. et al. 2006, Science 311, 201

Rodriguez, S. et al. 2003, Icarus 164, 213

Sanchez-Lavega, A. et al. 2004, American Journal of Physics 72, 767

Sandford, S.A. & Allamandola, L.J. 1993, Icarus 106, 478

Schriver-Mazzuoli, L. et al. 2003, Journal of Molecular Structure 644, 151

Signorell, R. 2003a, Molecular Physics 101, 3385

Signorell, R. 2003b, Journal of Chemical Physics 118, 2707

Signorell, R. & Kunzmann, M.K. 2003, Chemical Physics Letters 371, 260

Signorell, R. et al. 2006, Journal of Physical Chemistry A 110, 2890

Signorell, R. & Jetzki, M. 2007, Physical Review Letters 98, 013401

Signorell, R. & Jetzki, M. 2008, Faraday Discussions 137, 51

Sigurbjörnsson, Ó.F. & Signorell, R. 2008, Physical Chemistry Chemical Physics 10, 6211

Sigurbjörnsson, Ó.F. et al. 2009, Annual Review of Physical Chemistry 60, 127

Smith, B.A. et al. 1989, Science 246, 1422

Snyder, R.G. & Schachtschneider, J.H. 1963, Spectrochimica Acta 19, 85

Snyder, R.G. 1967, Journal of Chemical Physics 47, 1316

Spencer, J.R. et al. 2005, Icarus 176, 283

Taraschewski, M. et al. 2005, Journal of Physical Chemistry A 109, 3337

Thalladi, V.R. & Boese, R. 2000, New Journal of Chemistry 24, 579

Tokano, T. et al. 2006, Nature 442, 432

Tomasko, M.G. et al. 2005, Nature 438, 765

Wang, C.C. et al. 2009, Journal of Physical Chemistry A 113, 11129

Wang, C.C. et al. 2010, Astrophysical Journal Letters 712, 40

White, J.U. 1942, Journal of the Optical Society of America 32, 285